

## Article

# Numerical Study on the Influence of Well Layout on Electricity Generation Performance of Enhanced Geothermal Systems

Yuchao Zeng <sup>1</sup>, Fangdi Sun <sup>2</sup> and Haizhen Zhai <sup>3,\*</sup>

<sup>1</sup> National-Regional Joint Engineering Research Center for Soil Pollution Control and Remediation in South China, Guangdong Key Laboratory of Integrated Agro-Environmental Pollution Control and Management, Institute of Eco-Environmental and Soil Science, Guangdong Academy of Sciences, Guangzhou 510650, China; zengyuc@126.com

<sup>2</sup> School of Geography and Remote Sensing, Guangzhou University, Guangzhou 510006, China; sfd\_geo@gzhu.edu.cn

<sup>3</sup> Guangzhou Institute of Energy Conversion, Chinese Academy of Sciences, Guangzhou 510640, China

\* Correspondence: zhaih@ms.giec.ac.cn

**Abstract:** The energy efficiency of the enhanced geothermal system (EGS) measures the economic value of the heat production and electricity generation, and it is a key indicator of system production performance. Presently there is no systematic study on the influence of well layout on the system energy efficiency. In this work we numerically analyzed the main factors affecting the energy efficiency of EGS using the TOUGH2-EOS1 codes at Gonghe Basin geothermal field, Qinghai province. The results show that for the reservoirs of the same size, the electric power of the three horizontal well system is higher than that of the five vertical well system, and the electric power of the five vertical well system is higher than that of the three vertical well system. The energy efficiency of the three horizontal well system is higher than that of the five vertical well system and the three vertical well system. The reservoir impedance of the three horizontal well system is lower than that of the three vertical well system, and the reservoir impedance of the three vertical well system is lower than that of the five vertical system. The sensitivity analysis shows that well spacing has an obvious impact on the electricity production performance; decreasing well spacing will reduce the electric power, reduce the energy efficiency and only have very slight influence on the reservoir impedance. Fracture spacing has an obvious impact on the electricity production performance; increasing fracture spacing will reduce the electric power and reduce the energy efficiency. Fracture permeability has an obvious impact on the electricity production performance; increasing fracture permeability will improve the energy efficiency and reduce the reservoir impedance.

**Keywords:** energy efficiency; horizontal well; enhanced geothermal system; well layout; vertical well



**Citation:** Zeng, Y.; Sun, F.; Zhai, H. Numerical Study on the Influence of Well Layout on Electricity Generation Performance of Enhanced Geothermal Systems. *Processes* **2021**, *9*, 1474. <https://doi.org/10.3390/pr9081474>

Academic Editor: Tohid N. Borhani

Received: 11 June 2021

Accepted: 20 August 2021

Published: 23 August 2021

**Publisher's Note:** MDPI stays neutral with regard to jurisdictional claims in published maps and institutional affiliations.



**Copyright:** © 2021 by the authors. Licensee MDPI, Basel, Switzerland. This article is an open access article distributed under the terms and conditions of the Creative Commons Attribution (CC BY) license (<https://creativecommons.org/licenses/by/4.0/>).

## 1. Introduction

### 1.1. Background

Enhanced geothermal systems employ artificial circulating water or CO<sub>2</sub> to extract heat from subsurface fractured hot dry rock (HDR) at depths of 3~10 km, and the produced heat is mainly used for electricity generation [1]. The EGS resource is more stable and concentrated, and very suitable for producing base-load electric power with nearly no pollution emission and a high utilization efficiency [1–3]. In China, the total EGS resource reserve within 3–10 km depths amounts to 20.90 M EJ; if 2% is taken as the recoverable fraction, the recoverable EGS resource amounts to 4400 times total annual energy consumption in 2010 [4].

Study on the performance analysis of the EGS can provide guidance for optimization design of the power plant, thus the performance analysis is a key problem for research, development and design of EGS power plant [1]. There are mainly two methods to research the performance of EGS: field test and numerical simulation [1]. The field test

of EGS originates from the pioneering Fenton Hill test conducted by the Los Alamos National Laboratory in USA in 1974. Later, industrial field tests of EGS were successively conducted in the UK, Germany, France and Japan, and important progress has been made from different aspects [1]. Presently there are four main sites, which are doing the EGS field test all over the world. (1) Soultz in France: The test began in 1987 and has been conducted up to now. Presently the Soultz EGS adopts three vertical wells of 5 km depth to extract the geothermal heat, and the surface power station uses the ORC (Organic Rankine Cycle) system at a capacity of 1.5 MW<sub>e</sub>. The Soultz EGS starts to generate electricity from June 2008 [5]. (2) Desert Peak in USA: Well 27–15 was originally drilled to about 1771 m, and the final injectivity qualifies it as commercial injector [6]. (3) Landau in Germany: The Landau commercial power plant is based on a multi-horizon-concept, and it aims to produce hot water from a fault system in the Buntsandstein, Perm and the granitic basement. It is able to deliver about 3 MW<sub>e</sub> and about 4 MW<sub>th</sub> [7]. (4) Cooper Basin in Australia: The injection well of Habanero-1 was drilled to the depth of 4421 m in 2003; later, the production well of Habanero-2 was drilled to 4358 m depth in 2004 [1]. The important information about the mentioned EGS projects are listed in Table 1.

**Table 1.** Important ongoing EGS fields all over the world [1,5–7].

Project Name	Location	Reservoir Temperature (°C)	Reservoir Depth (km)	Well Design	Generating Capacity (MW <sub>e</sub> )
Soultz EGS	France	200	5	Three vertical wells	1.5
Desert Peak EGS	USA	210	1.771	Two vertical wells	1.7
Landau EGS	Germany	160	2.1~2.2	Two vertical wells	3
Cooper Basin	Australia	250	4	Two vertical wells	6

Field testing of EGS is time-consuming, very difficult and expensive, while numerical simulation is very fast, quite easy and cheap, with the numerical simulation studies of EGS reservoirs having achieved important progress recently [8–12]. The fractured EGS reservoir is not only a heat storage, but also a heat exchanger; the numerical simulation of EGS reservoir mainly concerns two aspects: fluid flow and heat transfer. In the aspect of fluid flow, the representation method of the fracture system in the fractured reservoir is mainly concerned. The common used methods for fracture representation include two types [13–15]. The DFN method analyzes the fracture spacing, aperture and orientation to establish a fracture network model [13–15]. In the aspect of heat transfer, based on the number of equations describing the temperature field of fluid and solid rock, the models include the local thermodynamic equilibrium (LTE) type and the local thermodynamic non-equilibrium (LTNE) type [16]. The LTE model assumes that the thermodynamic equilibrium between water and rock can be quickly established, and only uses one equation to describe the temperature field of rock and water. The LTNE model regards the temperature difference between the water and rock, and uses two different equations to describe the temperature field of rock and water, respectively [16–18].

The EPM method is mainly used when the fracture spacing is small [8–12]. Zeng et al. adopted the EPM method to analyze the heat production performance of EGSs via two horizontal wells and a single vertical fracture and found that using two horizontal wells can obtain better performance, while using a single vertical fracture can only obtain poor performance [13,14]. Zeng et al. used the EPM method to analyze the electricity generation performance of EGSs via a single horizontal well [15], multi vertical wells [19], multi horizontal wells [20] and a single vertical well [21]. Zeng et al. used the EPM method to analyze the factors affecting heat production of EGS reservoirs [2] and ranked the relative importance of the factors through orthogonal experimental design [22]. Watanabe et al. employed the EPM approach to conduct an uncertainty analysis of thermo-hydro-mechanical coupled processes based on the EGS data from the Urach Spa and Falkenberg sites in Germany [23]. McDermott et al. utilized the EPM to research impacts of the coupling interaction among hydrologic-thermal-mechanical-chemical processes on production performance of EGS [24].

Birdsell et al. adopted the EPM to establish a three-dimensional model, and it is used to predict long-term performance [25,26]. Hu et al. used the EPM method to establish a novel fully coupled fluid flow and geomechanical model of TOUGH2-EGS [27].

When the average fracture spacing is larger than 10 m, the temperature difference between water and rock must be considered, thus the DPM or MINC method is more reasonable [8–12]. Sanyal et al. used the DPM method to analyze the electricity production prospects from EGSs based on the geological data at Desert Peak geothermal field, and found that increasing permeability without increasing matrix-to-fracture heat transfer area has little effect in heat recovery [28]. Gelet et al. established a thermo-hydro-mechanical coupled model based on the DPM method and analyzed the impacts of fracture spacing on the heat production performance of EGS [29–32]. Benato et al. employed the DPM simulator TFReact to study the mechanisms affecting permeability evolution [6]. Pruess et al. used the MINC method to study the heat production performance of CO<sub>2</sub> EGS [33,34]. Spycher et al. adopted the MINC method to establish a phase-partitioning model for CO<sub>2</sub>-Brine mixtures and employed this novel model to study the production performance of a CO<sub>2</sub> EGS [35,36]. Zeng et al. used the MINC method to study the electricity generation potential from fractured granite reservoir at Yangbajing geothermal field [37,38].

If the data of reservoir fracture orientation and spacing are available, we can use the DFN model [8–12]. Kolditz et al. used the DFN method to study heat transfer characteristics during water circulating through fractured rock in Rosemanowes [39–43]. Baujard et al. employed the DFN method to analyze the influence of fluid density on the stimulated volume and pressure distribution in the Soultz EGS reservoir [44–46].

Recently, the development and application of the LTNE models in modeling EGS reservoirs are increasing. Shaik et al. established an LTNE model for modeling heat extraction in fractured geothermal reservoirs considering characteristic properties of fractures [16]. Jiang et al. carefully considered the LNTE effect in the EGS reservoirs, and regarding the dense fracture network as an equivalent porous media they established a LNTE model for the subsurface heat exchange [17,18]. Gelet et al. and Sun et al. considered the LNTE effect in their newly built DPM and DFN model, respectively [30,31,46,47]. Chen et al. employed the LNTE model to analyze the heat production performance of EGS reservoirs, and they made many important progress [47–49]. Cao et al. used the LNTE model to investigate the variable thermophysical properties of heat transfer fluid and the thermal-hydraulic-mechanical processes in EGS reservoirs [50,51].

Though the numerical modeling of EGS reservoirs have attained great progress, most models only consider the change of production temperature and thermal power versus time, and the change of system energy efficiency versus time is not included. The energy efficiency of EGS is defined as the ratio of produced electric power to internally consumed power, it determines the commercial value of development of EGS reservoirs, and it is also the most important parameter measuring the electricity generation performance [2]. Based on the previous studies, in this work we define and deduce the computational formula of the energy efficiency of EGS, and carefully analyze the influence of well layout, fracture spacing and permeability on the system energy efficiency. These will provide guidance for future improving the energy efficiency of EGSs.

### 1.2. Research Objectives

Previous studies have proven that, via two horizontal wells at the Gonghe Basin geothermal field, the system can attain electric power of 3.59–3.05 MW and an energy efficiency of 62.4–31.0 during 30 years [38]. This has laid a good foundation for future development of EGS resources here. The research objectives of this work are to systematically analyze the numerous factors affecting the electricity generation performance of EGS, especially the well layout, to find the main approaches to improve the energy efficiency, and to raise methods to optimize the system performance.

The novelty of this work mainly lies in two features: first, we used the MINC method to characterize the fracture system; second, we analyzed the affecting factors of the energy

efficiency from two aspects of well layout and fracture spacing and permeability, and the analyses are more systematic and profound.

## 2. Numerical Method

### 2.1. Physical Model

In order to analyze the impact of well layout on the production performance of EGS, in this study we consider heat mining schemes via vertical wells and horizontal wells, respectively. For vertical well systems, we consider three vertical wells and five vertical wells (an injector at the center and four production wells at corners of a square), respectively, as shown in Figure 1. For horizontal well systems, we consider the three horizontal wells (an injector at bottom flanked by two production well at top on each side), as shown in Figure 2. We mainly investigate the energy efficiency of the three systems, and analyze the influence of well spacing, fracture spacing and permeability on the energy efficiency. The gray areas in Figures 1 and 2 show the computational domain because of symmetry.

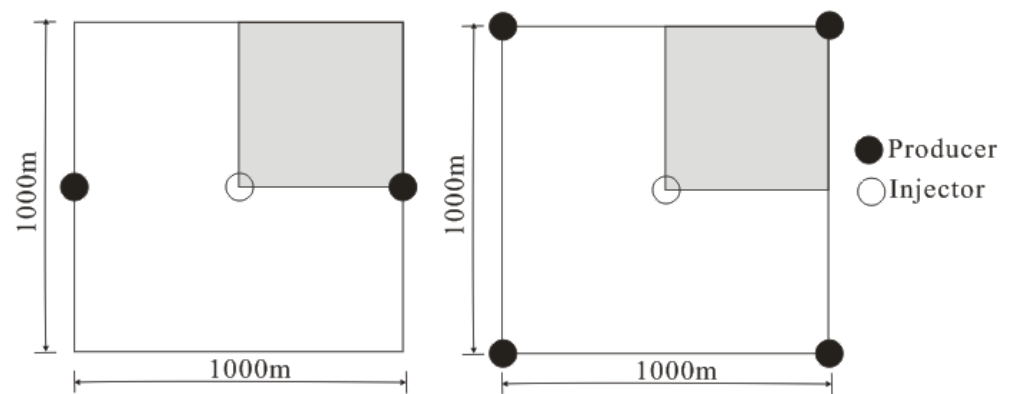


Figure 1. The EGSs of three vertical wells and five vertical wells.

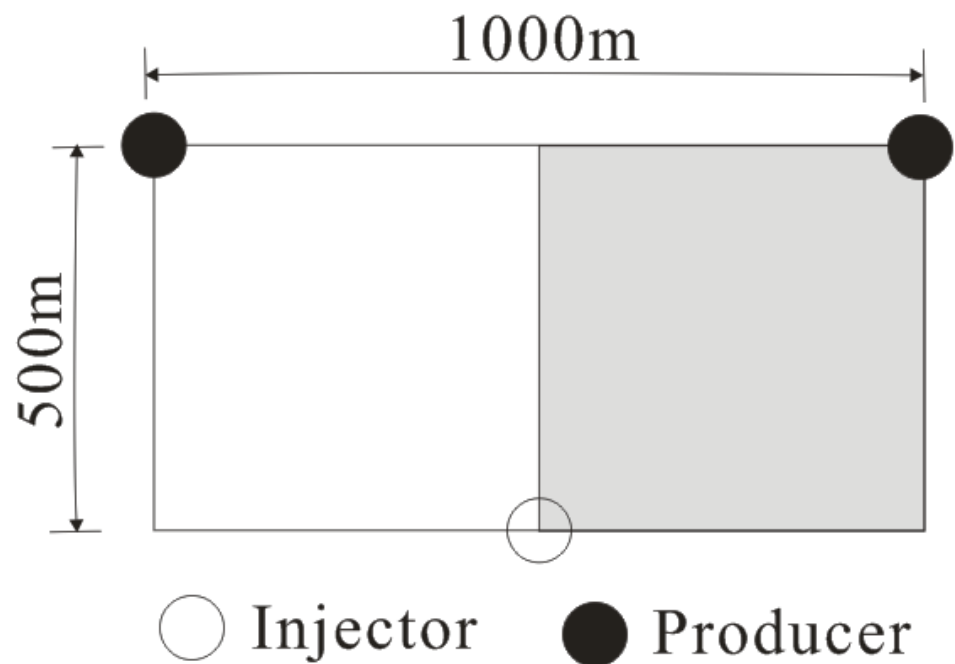


Figure 2. The EGS of three horizontal wells.

In order to reduce reservoir impedance and water loss [2], the production well is maintained against a constant backpressure, and the bottom hole pressure  $P_{pro}$  at the production well is maintained constant via a downhole pump. An injection pump is

installed on the ground, and the injection rate  $q$  is kept unchanged. This kind of water circulating method accords with the requirement of long term production of EGS [2]. Ignoring the water loss in the reservoir, the production rate  $q_{\text{pro}}$  equals to the injection rate  $q_{\text{inj}}$ :  $q_{\text{inj}} = q_{\text{pro}} = q$ . The water circulation rate  $q$  depends on the injection pressure  $P_{\text{inj}}$  at the bottom of the injection well, and it rises with increasing injection pressure. According to the experience of oil and gas industry,  $P_{\text{inj}}$  must be lower than the minimum formation principal stress. In this study we assume that  $P_{\text{inj}}$  be kept lower than an upper limit  $P_{\text{max}}$ :

$$P_{\text{inj}} < P_{\text{max}} \quad (1)$$

where  $P_{\text{max}} = fP_{W0}$ ;  $f = 1.2$  is a safety factor, and  $P_{W0}$  is the initial formation pressure at the wellbore [13].

## 2.2. Mathematical Model

In this study, we employed the TOUGH2-EOS1 codes to solve the mathematical models corresponding to the above conceptual models [52]. The corresponding governing equations are listed in the user's manual of the TOUGH2, which we did not repeat here [52]. The comparison with the experimental and analytical results proves that the computational results of the TOUGH2 are accurate and reliable [52]; accordingly, these codes have been widely used in the simulation of heat mining. Below we will deduce the computational formula of energy efficiency of the EGS, and this is the core content of this work.

If the water circulation rate of an EGS is  $q$ , the injection specific enthalpy is  $h_{\text{inj}}$ , the production specific enthalpy is  $h_{\text{pro}}$ , then for the system the thermal power can be calculated as (2):

$$W_h = q(h_{\text{pro}} - h_{\text{inj}}) \quad (2)$$

If the heat rejection temperature of the EGS power plant is  $T_o$ , and the production temperature at the wellhead of the production well is  $T_{\text{pro}}$ , then the fraction  $f_R$  is (3) according to the second law of thermodynamics:

$$f_R = 1 - \frac{T_o}{T_{\text{pro}}} \quad (3)$$

The electric power  $W_e$  is (4) [2]:

$$W_e = 0.45f_R W_h = 0.45q(h_{\text{pro}} - h_{\text{inj}})\left(1 - \frac{T_o}{T_{\text{pro}}}\right) \quad (4)$$

The internal energy consumption  $W_p = W_{p1} + W_{p2}$ , includes  $W_{p1}$  and  $W_{p2}$  [13,14]:

$$W_{p1} = \frac{q(P_{\text{inj}} - \rho g h_1)}{\rho \eta_p} \quad (5)$$

$$W_{p2} = \frac{q(\rho g h_2 - P_{\text{pro}})}{\rho \eta_p} \quad (6)$$

where  $h_1$  is the depth of the injection well,  $h_2$  is the depth of production well, and  $\eta_p = 80\%$  is the pump efficiency [13,14]. Consequently the internal energy consumption  $W_p$  is (7):

$$W_p = W_{p1} + W_{p2} = \frac{q(P_{\text{inj}} - P_{\text{pro}}) - \rho q g (h_1 - h_2)}{\rho \eta_p} \quad (7)$$

The energy efficiency  $\eta$  can be calculated as Equation (8):

$$\eta = \frac{W_e}{W_p} = \frac{0.45\rho\eta_p(h_{\text{pro}} - h_{\text{inj}})(1 - T_o/T_{\text{pro}})}{(P_{\text{inj}} - P_{\text{pro}}) - \rho g(h_1 - h_2)} \quad (8)$$

The flow impedance in the reservoir is (9) [2]:

$$I_R = \frac{P_{inj} - P_{pro}}{q} \quad (9)$$

### 2.3. Domain, Grid and Parameters

For the vertical well systems, the horizontal dimensions are  $500 \times 500$  m and the thickness is 500 m for the simulated domain. We have used the reservoir domain of the same size in order to be convenient for comparison and analyzation. For the simulated domain of  $500 \times 500 \times 500$  m dimensions, it is evenly divided into 20 gridblocks in the horizontal dimensions, and the width of each gridblock is 25 m; it is evenly divided into 20 gridblocks in the vertical dimension, and the height of each gridblock is also 25 m. Thus there are total  $20 \times 20 \times 20 = 8000$  gridblocks for the simulated domain of the vertical well system. Figure 3 shows the simulated domain and three-dimensional grid for the vertical well system. For the horizontal well system, because of the symmetry along the well length, only 10 m long well interval of the domain is simulated, and the actual simulated domain is  $500 \times 500 \times 10$  m. Consequently, the thermal power and electric power of the 1000 m length is 100 times that of the simulated domain. For the three horizontal well system, there are total  $20 \times 1 \times 20 = 400$  gridblocks for the simulated domain. Figure 4 shows the simulated domain and two-dimensional grid for the horizontal well system. The reservoir domain is divided into five continua; the volume fraction of the outmost continuum is 0.02; the other four continua represent the rock matrix, and their volume fraction is 0.08, 0.2, 0.35 and 0.35 in sequence [37]. After this partition, there are total  $8000 \times 5 = 40,000$  gridblocks for the vertical well system, and total  $400 \times 5 = 2000$  gridblocks for the horizontal well system.

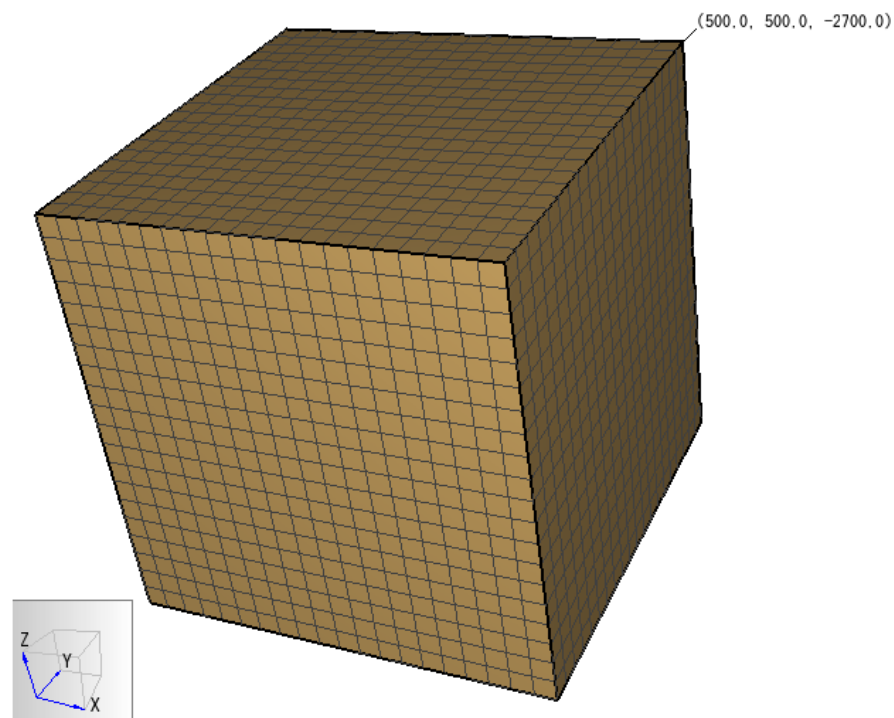


**Figure 3.** The simulated domain and three-dimension grid for the vertical well system.

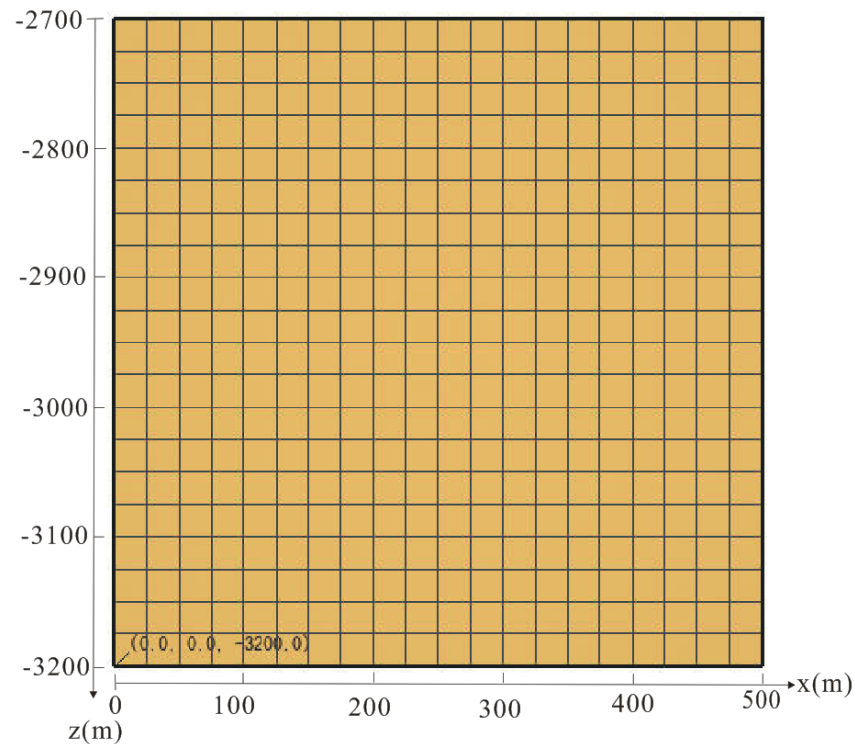


**Figure 4.** The simulated domain and two-dimensional grid for the horizontal well system.

The system parameters have significant influence on the heat production performance [2]. The property parameters and condition parameters of the geothermal filed are listed in Table 2 [37], and using the practical reservoir parameters makes the computation and analyzation more reliable.

**Table 2.** EGS reservoir properties at well DR3 in the Gonghe Basin geothermal area [37].

Parameter	Value
Rock grain density	2650 kg/m <sup>3</sup>
Rock specific heat	1000 J/(kg·K)
Rock heat conductivity	2.50 W/(m·K)
Fracture system volume fraction	2%
Fracture spacing	50 m
Porosity in fracture system	0.5
Porosity in matrix	$1.0 \times 10^{-5}$
Permeability in fracture system	$50 \times 10^{-15}$ m <sup>2</sup>
Permeability in matrix	$1.0 \times 10^{-18}$ m <sup>2</sup>
Injection temperature	60 °C (277.221 kJ/kg)
Bottomhole production pressure	24.0 MPa
Productivity index	$5.0 \times 10^{-12}$ m <sup>3</sup>

#### 2.4. Boundary and Initial Conditions

The initial temperature is 180 °C, and the initial pressure is  $P = -0.0088z + 3.24$ (MPa) [37]. The saturated vapor pressure corresponding to 180 °C of pure water is 1.00 MPa, far lower than the bottomhole production pressure of 24.0 MPa, thus the water is maintained as liquid in the reservoir and well.

### 3. Results and Discussion

#### 3.1. The Determination of Water Production Rate

The maximum available water production rate of the system can be determined based on (1) and the production temperature drop. Under the maximum available water

production rate, the system can achieve maximum electric power and minimum reservoir impedance [2], and this makes the system performance optimal. Consequently, in this study the water production rates of the systems all take the maximum water production rate. The injection pressure  $P_{inj}$  rises with increasing water production rate, while the production temperature  $T_{pro}$  decreases with increasing water production rate. According to the principle that the  $P_{inj}$  is lower than the  $P_{max}$  and the production temperature drop is lower than 10%, through adjusting the water production rate of every case we can determine the optimal water production rate of every system [2].

For the vertical well system, in this study the injection perforated interval is located at the depth of  $-3200\sim-3150$  m. The coordinate of the midpoint of the injection perforated interval is  $z = -3175$  m, corresponding to an initial pressure of  $P_{W0} = 31.18$  MPa, thus the maximum pressure of the  $P_{inj}$  is  $P_{max} = 1.2 P_{W0} = 37.416$  MPa, and during the production period the injection pressure should meet:  $P_{inj} < P_{max} = 37.416$  MPa. The bottomhole pressure at the production well is maintained unchanged, and the maximum production pressure drawdown is 3.40 MPa [28]. The production perforated interval is located at the depth of  $-2750\sim-2700$  m; the coordinate of the midpoint of the production perforated interval is  $z = -2725$ , corresponding to an initial pressure of 27.22 MPa, thus the available minimum bottomhole pressure  $P_{pro}$  is  $(27.22 \text{ MPa} - 3.40 \text{ MPa}) = 23.82$  MPa. For easy computation, in this study the bottomhole production pressure  $P_{pro}$  is maintained at 24.0 MPa.

For the horizontal well system, the injection well is located at  $z = -3175$  m, corresponding to an initial pressure of  $P_{W0} = 31.18$  MPa, thus during the production period the injection pressure should meet:  $P_{inj} < P_{max} = 1.2 P_{W0} = 37.416$  MPa. The production well is located at  $z = -2725$  m, corresponding to an initial pressure of 27.22 MP.

Table 3 shows the well layout and water production rate of every simulation case, and Figure 5 shows the change of injection pressure versus time of the three well layouts. During the production period, the heat in the rock is gradually extracted out, the reservoir temperature gradually declines, the water viscosity gradually increases and this makes the injection pressure gradually increasing [2]. According to the principle that during the production period  $P_{inj} < P_{max} = 37.416$  MPa and the production temperature drop is lower than 10%, we can determine that for the three vertical well system the water production rate is 32 kg/s in the simulated domain and the total water production rate is 128 kg/s, corresponding to case 2. For the five vertical well system, the water production rate is 32.6 kg/s in the simulated domain and the total water production rate is 130.4 kg/s, corresponding to case 4. For the three horizontal well system, the water production rate is 1 kg/s, corresponding to case 9. Consequently, for reservoirs of the same size, using the horizontal well can obtain maximum water production rate, the water production rate of vertical well system is much lower, and the water production rate of five vertical well system is higher than that of the three vertical well system. This is because the length of the perforated interval of the horizontal well is 1000 m, much longer than that of the vertical well of 50 m, thus the horizontal well system can obtain higher water production rate under lower injection pressure.

**Table 3.** The well layout and water production rate corresponding to every simulation case.

Case Number	Well Layout	Simulated Water Production Rate (kg/s)	Total Water Production Rate (kg/s)
1	Three vertical wells	20	80
2	Three vertical wells	32	128
3	Three vertical wells	26	104
4	Five vertical wells	32.6	130.4
5	Five vertical wells	22	88
6	Five vertical wells	28	112
7	Three horizontal wells	0.5	100
8	Three horizontal wells	0.75	150
9	Three horizontal wells	1.0	200

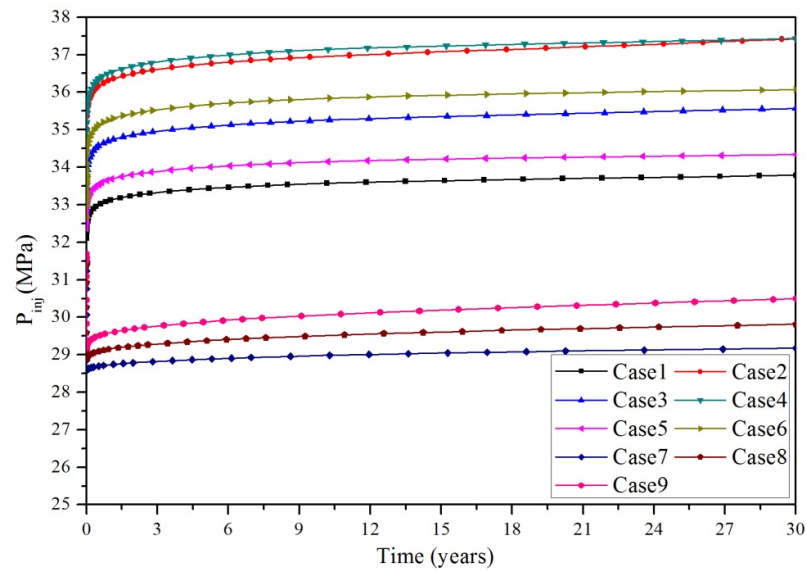


**Figure 5.** The injection pressure versus time in every case.

### 3.2. The Influence of the Well Layout

For the above determined water production rate, Figure 6 shows the change of production temperature versus time under different well layouts. Figure 6 indicates that for the reservoir of  $1000 \times 1000 \times 500$  m size, the production temperature via three vertical wells gradually declines from 180 to 162 °C during the 30 years; the production temperature via five vertical wells declines from 180 to 176.8 °C, and the production temperature via three horizontal wells declines from 180 to 162.2 °C. It can be easily found that the temperature drops of the three well layouts are all within 10%, and the selected cases all meet the engineering requirements [2]. The production temperature via five vertical wells is higher than that via three vertical wells, this is because in the five vertical well system the distance between the injection well and production well is greater than that in the three vertical well system, and the reservoir can provide more heat in the same time. The production temperature via three horizontal wells is in between that via three vertical wells and five vertical wells, and this shows that there is no significant difference of the production temperature between the vertical well system and horizontal well system. This agrees with previous studies from Zeng et al. [13,20].

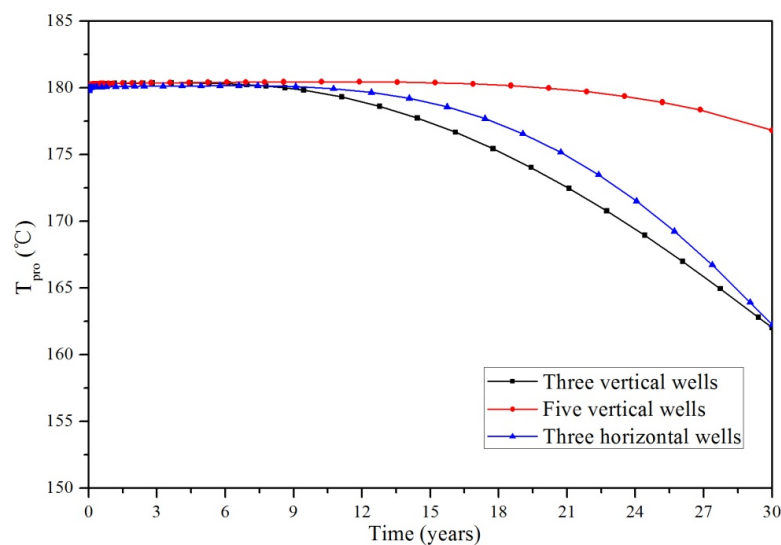


**Figure 6.** The change of production temperature versus time under different well layouts.

In the calculation of the electric power in Equation (4) at Gonghe Basin geothermal field, the heat rejection temperature is  $T_0 = 4.1\text{ }^\circ\text{C} = 277.25\text{ K}$  [37]. Figure 7 shows the change of the electric power versus time under different well layouts. The electric power gradually declines from 11.13 to 8.81 MW via three vertical wells, and it declines from 11.33 MW to 10.92 MW during the 30 years via five vertical wells. The electric power gradually declines from 17.36 to 13.79 MW via three horizontal wells during the 30 years. Figure 7 shows that for reservoirs of the same size of  $1000 \times 1000 \times 500\text{ m}$ , the electric power via three horizontal wells is higher than that via five vertical wells, and the electric power via five vertical wells is higher than that via three vertical wells. Based on Equation (4), main factors influencing the electric power is water production rate  $q$  and the production temperature  $T_{\text{pro}}$ . As stated above, because the sequence of water production rate is three horizontal wells > five vertical wells > three vertical wells, the production temperature difference is very small, thus the electric power is mainly determined by the water production rate, and the three horizontal well system obtains highest electric power and the three vertical well system obtains lowest electric power.

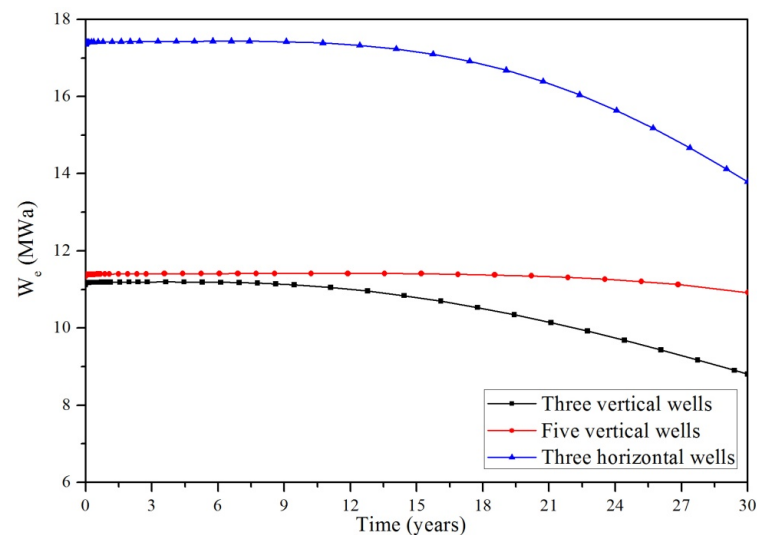


**Figure 7.** The change of electric power versus time under different well layouts.

In the calculations of energy efficiency in this study, the water density  $\rho$  in Equations (5)–(8) changes with water pressure and temperature. In previous studies from Zeng et al., the average value of  $\rho$  is adopted to perform the calculations in Equations (5)–(8), and the results can meet the precision requirements [2,13–15,19–22]. Under above three reference cases, the maximum value of the  $\rho$  is  $1000\text{ kg/m}^3$ , the minimum value of the  $\rho$  is  $900\text{ kg/m}^3$ , thus in this work the average value of  $\rho$  is  $950\text{ kg/m}^3$  and this value is used for Equations (5)–(8). In this study  $h_1 = 3175.0\text{ m}$ ,  $h_2 = 2725.0\text{ m}$ , thus  $h_1 - h_2 = 450\text{ m}$ . Figure 8 shows the change of the energy efficiency versus time under different well layouts. We can find that for the three vertical well system, the energy efficiency declines from 14.15 to 5.66 during the 30 years; for the five vertical well system, the energy efficiency declines from 14.06 to 6.88 during the 30 years; for the three horizontal well system, the energy efficiency gradually declines from 66.49 to 22.72 during the 30 years. According to equation (8), because the  $T_{\text{pro}}$  gradually declines, the  $P_{\text{inj}}$  gradually increases, thus the system energy efficiency gradually decreases [2], and the energy efficiency has no connection with water production rate  $q$ . Because the injection pressure of horizontal well system is far lower than that of vertical well system, the energy efficiency of horizontal well system is far higher than that of vertical well system. There is no significant difference of the energy efficiency between the three vertical well system and five vertical well system, because the  $T_{\text{pro}}$  and  $P_{\text{inj}}$  of both systems are very close.

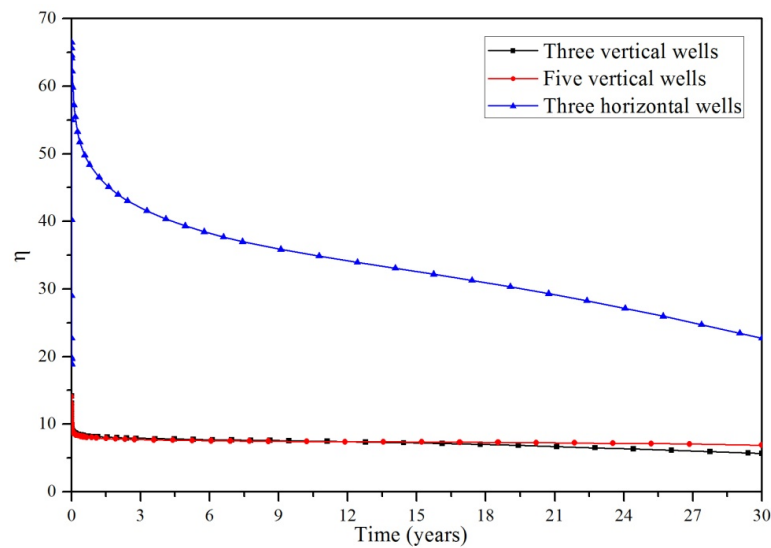


**Figure 8.** The change of energy efficiency versus time under different well layouts.

Figure 9 shows the change of reservoir impedance versus time under different well layouts. We can find that for the three vertical well system, the reservoir impedance gradually increases from 0.138 MPa/(kg/s) to 0.210 MPa/(kg/s) during the 30 years; for the five vertical well system, the reservoir impedance gradually increases from 0.273 MPa/(kg/s) to 0.412 MPa/(kg/s) during the 30 years; for the three horizontal well system, the reservoir impedance gradually increases from 0.052 MPa/(kg/s) to 0.065 MPa/(kg/s) during the 30 years. Garnish et al. have proposed that  $I_R$  should be lower than 0.1 MPa/(kg/s) during the production period, while Evans thought the limit value of  $I_R$  can be enlarged to 0.2 MPa/(kg/s) [2]. We can find that the reservoir impedance via three horizontal wells is lowest, and it can strictly meet the engineering requirement; the reservoir impedance via five vertical wells is highest. Because the perforation length of the horizontal well is much longer, this makes the water production rate much higher and injection pressure much lower, thus based on Equation (9) the horizontal well system can obtain lower reservoir impedance, and this is also biggest advantage of developing horizontal well technology [13,20]. For the three vertical well system and five vertical well system, there is no significant difference of the injection pressure; because the distance between the injection well and production well in the five vertical well system is much longer than that in the three vertical well system, the reservoir impedance via five vertical wells is much higher than that via three vertical wells.

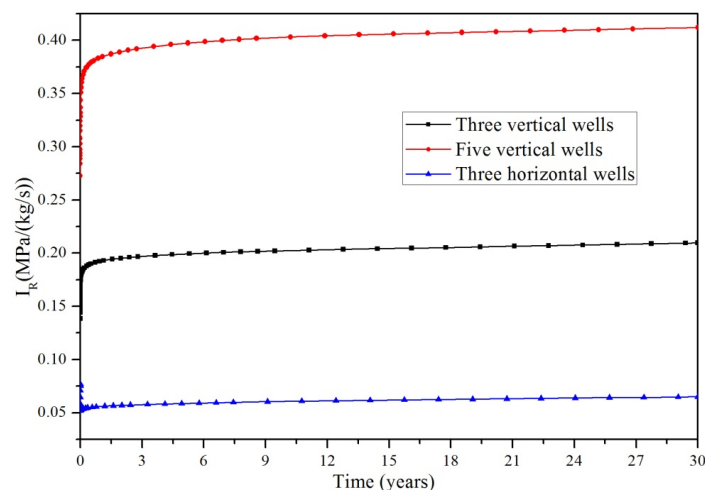


**Figure 9.** The change of reservoir impedance versus time under different well layouts.

### 3.3. Sensitivity Analysis

Based on the three base cases of above three well layouts, we further analyzed the influence of three important parameters on the system electricity generation performance: well spacing (WS), fracture spacing (D) and fracture permeability (K). Based on the base cases, we only changed one parameter to investigate its influence on the system performance, and these includes: (1) decreasing the WS from 500 to 400 m; (2) increasing the D from 50 to 75 m; (3) increasing the K from 50 mD to 75 mD. Figures 10–12 show the sensitivity of electric power, energy efficiency and reservoir impedance to well spacing, fracture spacing and fracture permeability, respectively.

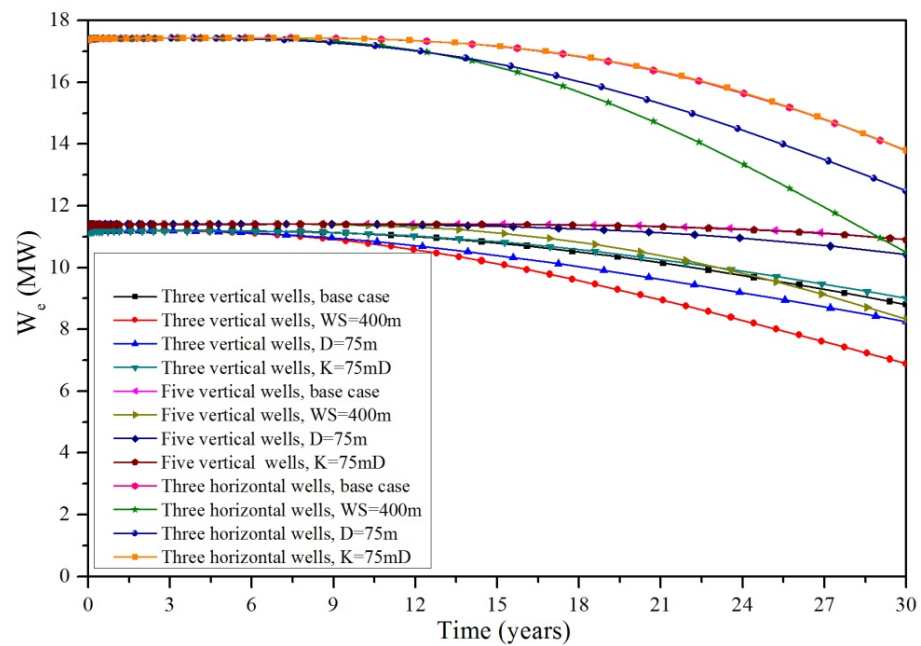


Figure 10. Sensitivity of electric power to main parameters.

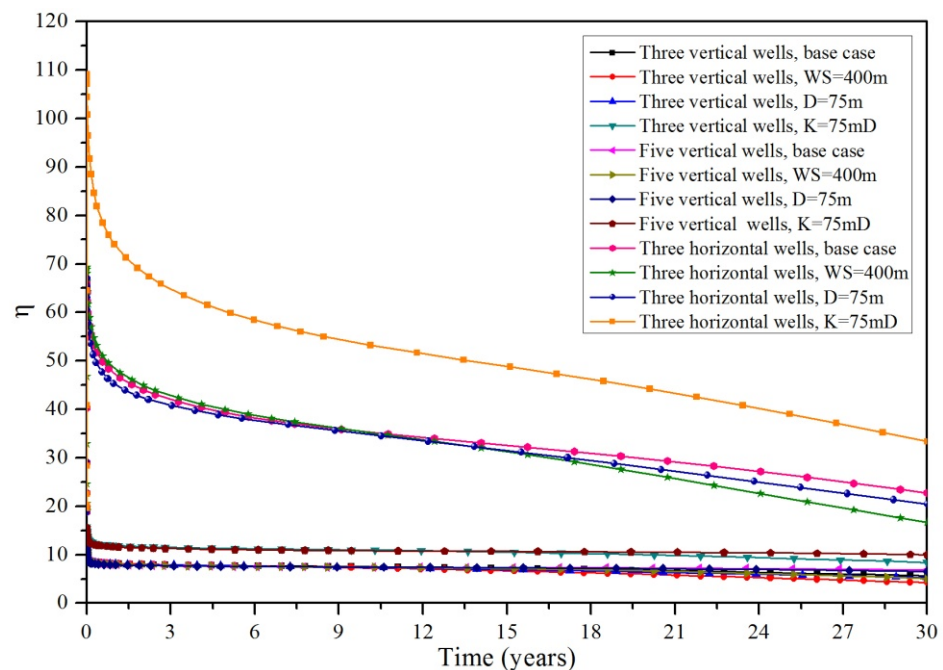
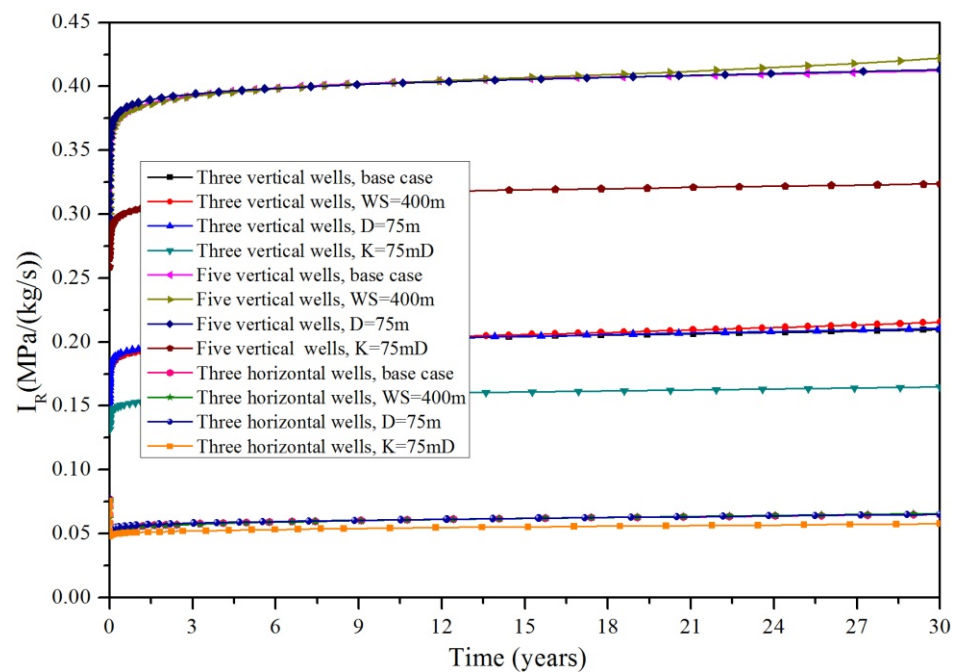


Figure 11. Sensitivity of energy efficiency to main parameters.



**Figure 12.** Sensitivity of reservoir impedance to main parameters.

### 3.3.1. Sensitivity to Well Spacing

Figure 10 shows that for the three vertical well system, decreasing well spacing from 500 to 400 m results in a drop of the electric power from 11.13~8.81 MW to 11.13~6.89 MW. For the five vertical well system and three horizontal well system, the decrease of well spacing also causes the drop of the electric power. This is mainly because lower well spacing obviously decreases the production temperature  $T_{pro}$  and production specific enthalpy  $h_{pro}$ , and this significantly decreases the electric power according to Equation (4). This shows that well spacing is an important controlling parameter for EGS power station design; for a given water production rate and injection temperature, the well spacing will significantly influence the electric power. Figure 11 shows that for the three vertical well system, decreasing well spacing from 500 to 400 m results in a drop of the energy efficiency from 14.15~5.66 to 14.15~4.26. It is the same for the five vertical well system and the three horizontal well system, the decrease of well spacing also causes drop of the energy efficiency. This is mainly because the decrease of well spacing significantly decreases the production temperature  $T_{pro}$  and production specific enthalpy  $h_{pro}$ , and this will obviously reduce the energy efficiency according to Equation (8). Figure 12 shows for the three vertical well system, decreasing the well spacing from 500 to 400 m has only very slight influence on the reservoir impedance. The five vertical well system and the three horizontal well system are the same, as the decrease of well spacing only causes very limited affect on the reservoir impedance. This proves that the well spacing is not a main factor affecting the reservoir impedance. Overall, the well spacing has a significant influence on the system production performance; within a certain range, decreasing well spacing will reduce the electric power, reduce the energy efficiency and have only very slight influence on the reservoir impedance.

### 3.3.2. Sensitivity to Fracture Spacing

Figure 10 shows that for three vertical well system, increasing the fracture spacing from 50 to 75 m results in a drop of the electric power from 11.13~8.81 MW to 11.13~8.25 MW. It is the same for the five vertical well system and the three horizontal well system, the increase of the fracture spacing also causes a decrease in the electric power. This is mainly because higher fracture spacing reduces the heat transfer area between the fractured rock and circulating water, and this will cause a reduction of thermal power and electric power

according to the computational formula of heat transfer. Figure 11 shows that for the three vertical well system, increasing the fracture spacing from 50 to 75 m results in a drop of the energy efficiency from 14.15~5.66 to 14.15~4.26. It is the same for the five vertical well system and the three horizontal well system, the increase of the fracture spacing also causes the reduction of the energy efficiency. This is mainly because the increase of fracture spacing obviously reduces the electric power, while it has only very slight influence on the injection pressure  $P_{inj}$ , this will obviously reduce the energy efficiency according to Equation (8). Figure 12 shows that for three vertical well system, increasing fracture spacing from 50 to 75 m has only very slight affect on the reservoir impedance. It is the same for the five vertical well system and the three horizontal well system, the increase of the fracture spacing also causes only very slight influence on the reservoir impedance. This is mainly because the reservoir impedance is mainly determined by water viscosity, the change of fracture spacing does not effectively influence the water viscosity, thus it has only very slight influence on the reservoir impedance. Overall, the fracture spacing has a significant influence on the production performance; within a certain range, increasing the fracture spacing will reduce the electric power, reduce the energy efficiency, and have only very slight affect on the reservoir impedance.

### 3.3.3. Sensitivity to Fracture Permeability

Figure 10 shows that for the three vertical well system, five vertical well system and three horizontal well system, increasing the fracture permeability from 50 to 75 mD has only very slight influence on the electric power. This is mainly because the fracture permeability has only very slight influence on the production temperature  $T_{pro}$  and production specific enthalpy  $h_{pro}$  within a certain range, thus it only has very slight effect on the electric power. This demonstrates that to control the system electric power we must adjust the well spacing and fracture spacing; within a certain range the change of fracture permeability has only very slight effect on the electric power. Figure 11 shows that increasing fracture permeability from 50 to 75 mD results in an increase of the energy efficiency from 14.15~5.66 to 15.66~8.41. It is the same for the five vertical well system and the three horizontal well system, the increase of the fracture permeability also causes the increase of the energy efficiency. This is mainly because the increase of fracture permeability obviously reduce the injection pressure  $P_{inj}$ , while it has only very slight effect on the production temperature  $T_{pro}$  and production specific enthalpy  $h_{pro}$ , thus this will obviously improve the system energy efficiency according to equation (8). Figure 12 shows that for the three vertical well system, increasing the fracture permeability from 50 to 75 mD results in a drop of the reservoir impedance from 0.138~0.210 MPa/(kg/s) to 0.131~0.165 MPa/(kg/s). It is the same for the five vertical well system and the three horizontal well system, as the increase of the fracture permeability also causes the reduction of reservoir impedance. This is mainly because higher fracture permeability effectively improves the water transmitting ability and obviously improves the flowing conditions of the fractures, thus significantly reducing the reservoir impedance. Overall, the fracture permeability has a significant influence on the system production performance; within a certain range, increasing the fracture permeability will improve the energy efficiency, reduce the reservoir impedance, and have only a very slight effect on the electric power.

### 3.4. Model Validation

TOUGH2-EOS1 codes employ the integral finite difference method to solve the balance equations of mass, momentum and energy, and the MINC method is an effective approach to simulate the water flow and heat transfer in fractured media [52]. The accuracy of the TOUGH2 codes has been proven by comparison with experiment measurement and theoretical analysis [52]. Using a reasonable grid and an appropriate model, the calculation results of TOUGH2 are reliable [2,13–15,52].

#### 4. Conclusions

In this study we analyzed the influence of well layout on the production performance of EGS and discussed the main factors affecting the production performance. The following conclusions are made.

- (1) For reservoirs of the same size of  $1000 \times 1000 \times 500$  m, the electric power via three horizon wells is higher than that via five vertical wells, and the electric power via five vertical wells is higher than that via three vertical wells.
- (2) For reservoirs of the same size of  $1000 \times 1000 \times 500$  m, because the injection pressure of the horizontal well system is far lower than that of the vertical well system, the energy efficiency of the horizontal well system is far higher than that of the vertical well system. There is no significant difference in the energy efficiency between the five vertical well system and the three vertical well system.
- (3) For reservoirs of the same size of  $1000 \times 1000 \times 500$  m, the reservoir impedance of the three horizontal well system is lowest, that of the five vertical well system is highest and that of the three vertical well system is in between.
- (4) The well spacing has an obvious impact on the system production performance; within a certain range, decreasing well spacing will reduce the electric power, reduce the energy efficiency and have only very slight influence on the reservoir impedance.
- (5) The fracture spacing has an obvious impact on the production performance; within a certain range, increasing the fracture spacing will reduce the electric power, reduce the energy efficiency, and have only very slight effect on the reservoir impedance.
- (6) The fracture permeability has an obvious impact on the system production performance; within a certain range increasing the fracture permeability will improve the energy efficiency, reduce the reservoir impedance, and have only very slight effect on the electric power.

**Author Contributions:** All the authors have contributed equally to the research and writing of this manuscript. All authors have read and agreed to the published version of the manuscript.

**Funding:** The study was financially supported by the GDAS Project of Science and Technology Development (2020GDASYL-20200102020, 2020GDASYL-20200102013, 2020GDASYL-20200301003, 2020GDASYL-20200402003, 2020GDASYL-20200302007, 2019GDASYL-0102002), Guangdong Foundation for Program of Science and Technology Research (2019B121205006, 2019B121201004), the National Natural Science Foundation of China (NSFC: 41930865) and Open Foundation of Key Laboratory of Natural Gas Hydrate, CAS (E0290206). We are also thankful for the support from the Northern Guangdong Soil Environment Observation and Research Station and the Guangdong Engineering Center of Non-point Source Pollution Control.

**Acknowledgments:** The authors are grateful for the comments by Nengyou Wu at the Qingdao Institute of Marine Geology, China Geological Survey, which significantly improved the manuscript.

**Conflicts of Interest:** The authors declare no conflict of interest.

#### Nomenclature

$g$	gravity, $9.80 \text{ m/s}^2$
$h$	well depth, m
$h_1$	depth of injection well, m
$h_2$	depth of production well, m
$h_{inj}$	injection specific enthalpy, $\text{kJ/kg}$
$h_{pro}$	production specific enthalpy, $\text{kJ/kg}$
$I_R$	reservoir impedance, $\text{MPa}/(\text{kg/s})$
$k$	reservoir permeability, $\text{m}^2$
$k_f$	fracture permeability, $\text{m}^2$
$k_m$	matrix permeability, $\text{m}^2$
$k_x$	intrinsic permeability along $x$ , $\text{m}^2$

$k_y$	intrinsic permeability along y, m <sup>2</sup>
$k_z$	intrinsic permeability along z, m <sup>2</sup>
$P$	pressure, MPa
$P_{\max}$	critical pressure, MPa
$P_{\text{inj}}$	injection pressure, MPa
$P_{\text{pro}}$	production pressure, MPa
$P_0$	bottomhole production pressure, MPa
$q$	water production rate, kg/s
$Q$	total water production rate, kg/s
$T$	temperature, °C
$T_0$	mean heat rejection temperature, 282.15 K
$T_{\text{pro}}$	production temperature, °C
$W_p$	electric power of pump, MW
$W_e$	electric power, MW
$x, y, z$	cartesian coordinates, m
$\phi$	reservoir porosity
$\eta$	energy efficiency
$\eta_p$	pump efficiency, 80%
$\rho$	water density, kg/m <sup>3</sup>

## References

1. Tester, J.W.; Livesay, B.; Anderson, B.J.; Moore, M.C.; Bathchelor, A.S.; Nichols, K.; Petty, S.; Toksoz, M.N.; Veatch, R.W.; Baria, R.; et al. *The Future of Geothermal Energy: Impact Enhanc. Geotherm. Syst. (EGS) United States 21st Century*; An Assessment by an MIT-led Interdisciplinary Panel; Massachusetts Institute of Technology: Cambridge, MA, USA, 2006.
2. Zeng, Y.C.; Tang, L.S.; Wu, N.Y.; Cao, Y.F. Analysis of influencing factors of production performance of enhanced geothermal system: A case study at Yangbajing geothermal field. *Energy* **2017**, *127*, 218–235. [[CrossRef](#)]
3. Zhao, Y.S.; Wan, Z.J.; Kang, J.R. *Introduction to HDR Geothermal Development*; Science Press: Beijing, China, 2004. (In Chinese)
4. Wang, J.; Hu, S.; Pang, Z.; He, L.; Zhao, P.; Zhu, C.; Rao, S.; Tang, X.; Kong, Y.; Luo, L.; et al. *Estimate of Geothermal Resources Potential for Hot Dry Rock in the Continental Area of China*; Science & Technology Review: Beijing, China, 2012; Volume 30, pp. 25–30. (Special issues) (In Chinese)
5. Genter, A.; Goerke, X.; Graff, J.; Cuenot, N.; Krall, G.; Schindler, M.; Ravier, G. Current status of the EGS soultz geothermal project (France). In Proceedings of the World Geothermal Congress 2010, Bali, Indonesia, 25–29 April 2010.
6. Benato, S.; Taron, J. Desert peak EGS: Mechanisms influencing permeability evolution investigated using dual-porosity simulator TFRact. *Geothermics* **2016**, *63*, 157–181. [[CrossRef](#)]
7. Schindler, M.; Baumgartner, J.; Gandy, T.; Hauffe, P.; Hettkamp, T.; Menzel, H.; Penzklfer, P.; Teza, D.; Tischner, T.; Wahl, G. Successful hydraulic stimulation techniques for electric power production in the Upper Rhine Graben, Central Europe. In Proceedings of the World Geothermal Congress 2010, Bali, Indonesia, 25–29 April 2010.
8. Pruess, K. Modelling of geothermal reservoirs: Fundamental processes, computer simulation, and field applications. In Proceedings of the 10th New Zealand Geothermal Workshop, Auckland, 15 August 1988.
9. Willis-richards, J.; Wallroth, T. Approaches to the modeling of HDR reservoirs: A review. *Geothermics* **1995**, *24*, 307–332. [[CrossRef](#)]
10. Hayashi, K.; Willis-Richards, J.; Hopkirk, R.J.; Niibori, Y. Numerical models of HDR geothermal reservoirs- a review of current thinking and progress. *Geothermics* **1999**, *28*, 507–518. [[CrossRef](#)]
11. Sanyal, S.K.; Butler, S.J.; Swenson, D.; Hardeman, B. Review of the state-of-the-art of numerical simulation of enhanced geothermal system. In Proceedings of the World Geothermal Congress; Kyushu-Tohoku, Japan, 28 May–10 June 2000.
12. O’Sullivan, M.J.; Pruess, K.; Lippmann, M.J. State of the art of geothermal reservoir simulation. *Geothermics* **2001**, *30*, 395–429. [[CrossRef](#)]
13. Zeng, Y.C.; Zheng, S.; Nengyou, W. Numerical simulation of heat production potential from hot dry rock by water circulating through two horizontal wells at Desert Peak geothermal field. *Energy* **2013**, *56*, 92–107. [[CrossRef](#)]
14. Zeng, Y.C.; Nengyou, W.; Zheng, S. Numerical simulation of heat production potential from hot dry rock by water circulating through a novel single vertical fracture at Desert Peak geothermal field. *Energy* **2013**, *63*, 268–282. [[CrossRef](#)]
15. Zeng, Y.; Nengyou, W.; Zheng, S. Numerical simulation of electricity generation potential from fractured granite reservoir through a single horizontal well at Yangbajing geothermal field. *Energy* **2014**, *65*, 472–487. [[CrossRef](#)]
16. Shaik, A.R.; Rahman, S.S.; Tran, N.H.; Tran, T. Numerical simulation of fluid-rock coupling heat transfer in naturally fractured geothermal system. *Appl. Therm. Eng.* **2011**, *31*, 1600–1606. [[CrossRef](#)]
17. Jiang, F.M.; Luo, L.; Chen, J.L. A novel three-dimensional transient model for subsurface heat exchange in enhanced geothermal systems. *Int. Commun. Heat Mass Transf.* **2013**, *41*, 57–62. [[CrossRef](#)]

18. Jiang, F.M.; Chen, J.L.; Huang, W.B.; Luo, L. A three-dimensional transient model for EGS subsurface thermo-hydraulic process. *Energy* **2014**, *72*, 300–310. [[CrossRef](#)]
19. Zeng, Y.; Zhan, J.; Nengyou, W. Numerical simulation of electricity generation potential from fractured granite reservoir through vertical wells at Yangbajing geothermal field. *Energy* **2016**, *103*, 290–304. [[CrossRef](#)]
20. Zeng, Y.; Zhan, J.; Nengyou, W. Numerical investigation of electricity generation potential from fractured granite reservoir by water circulating through three horizontal wells at Yangbajing geothermal field. *Appl. Therm. Eng.* **2016**, *104*, 1–15. [[CrossRef](#)]
21. Zeng, Y.; Zhan, J.; Nengyou, W. Numerical investigation of electricity generation potential from fractured granite reservoir through a single vertical well at Yangbajing geothermal field. *Energy* **2016**, *114*, 24–39. [[CrossRef](#)]
22. Zeng, Y.; Tang, L.; Nengyou, W.; Song, J.; Cao, Y. Orthogonal test analysis on conditions affecting electricity generation performance of an enhanced geothermal system at Yangbajing geothermal field. *Energies* **2017**, *10*, 2015. [[CrossRef](#)]
23. Watanabe, N.; Wang, W.Q.; McDermott, C.I.; Taniguchi, T.; Kolditz, O. Uncertainly analysis of thermo-hydro-mechanical coupled processes in heterogeneous porous media. *Comput. Mech.* **2010**, *45*, 263–280. [[CrossRef](#)]
24. McDermott, C.I.; Randriamanjatoa, A.R.; Tenzer, H.; Kolditz, O. Simulation of heat extraction from crystalline rocks: The influence of coupled processes on differential reservoir cooling. *Geothermics* **2006**, *35*, 321–344. [[CrossRef](#)]
25. Birdsell, S.; Robinson, B. A three-dimensional model of fluid, heat, and tracer transport in the Fenton Hill hot dry rock reservoir. In Proceedings of Thirteenth Workshop on Geothermal Reservoir Engineering, Stanford University, Stanford, CA, USA, 19–21 January 1988.
26. Cheng, W.-L.; Wang, C.-L.; Nian, Y.-L.; Han, B.-B.; Liu, J. Analysis of influencing factors of heat extraction from enhanced geothermal systems considering water losses. *Energy* **2016**, *115*, 274–288. [[CrossRef](#)]
27. Hu, L.T.; Winterfeld, P.H.; Fakcharoenphol, P.; Wu, Y.S. A novel fully-coupled flow and geomechanics model in enhanced geothermal reservoirs. *J. Pet. Sci. Eng.* **2013**, *107*, 1–11. [[CrossRef](#)]
28. Sanyal, S.K.; Butler, S.J. An analysis of power generation prospects from enhanced geothermal systems. In Proceedings of the World Geothermal Congress 2005, Antalya, Turkey, 24–29 April 2005; pp. 1–6.
29. Gelet, R.; Loret, B.; Khalili, N. A thermal-hydro-mechanical coupled model in local thermal non-equilibrium for fractured HDR reservoir with double porosity. *J. Geophys. Res.* **2012**, *117*, 1–23. [[CrossRef](#)]
30. Gelet, R.; Loret, B.; Khalili, N. Thermal recovery from a fractured medium in local thermal non-equilibrium. *Int. J. Numer. Anal. Method Geomech.* **2013**, *37*, 2471–2501. [[CrossRef](#)]
31. Taron, J.; Elsworth, D.; Min, K.B. Numerical simulation of thermal-hydrologic-mechanical-chemical processes in deformable, fractured porous media. *Int. J. Rock Mech. Min. Sci.* **2009**, *46*, 842–854. [[CrossRef](#)]
32. Taron, J.; Elsworth, D. Thermal-hydrologic-mechanical-chemical processes in the evolution of engineered geothermal reservoirs. *Int. J. Rock Mech. Min. Sci.* **2009**, *46*, 855–864. [[CrossRef](#)]
33. Pruess, K. Enhanced geothermal system (EGS) using CO<sub>2</sub> as working fluid—A novel approach for generating renewable energy with simultaneous sequestration of carbon. *Geothermics* **2006**, *35*, 351–367. [[CrossRef](#)]
34. Pruess, K. On production behavior of enhanced geothermal systems with CO<sub>2</sub> as working fluid. *Energy Convers. Manag.* **2008**, *49*, 1446–1454. [[CrossRef](#)]
35. Spycher, N.; Pruess, K. A phase-partitioning model for CO<sub>2</sub>-brine mixtures at elevated temperatures and pressures: Application to CO<sub>2</sub>-enhanced geothermal systems. *Transp. Porous Media* **2010**, *82*, 173–1796. [[CrossRef](#)]
36. Borgia, A.; Pruess, K.; Kneafsey, T.J.; Oldenburg, C.M.; Pan, L. Numerical simulation of salt precipitation in the fractures of a CO<sub>2</sub>-enhanced geothermal system. *Geothermics* **2012**, *44*, 13–22. [[CrossRef](#)]
37. Xu, T.F.; Yuan, Y.L.; Jia, X.F.; Lei, Y.D.; Li, S.T.; Feng, B.; Hou, Z.Y.; Jiang, Z.J. Prospects of power generation from an enhanced geothermal system by water circulation through two horizontal wells: A case study in the Gonghe Basin, Qinghai Province, China. *Energy* **2018**, *148*, 196–207. [[CrossRef](#)]
38. Zeng, Y.; Tang, L.; Wu, N.; Cao, Y. Numerical simulation of electricity generation potential from fractured granite reservoir using the MINC method at the Yangbajing geothermal field. *Geothermics* **2018**, *75*, 122–136. [[CrossRef](#)]
39. Kolditz, O.; Clauser, C. Numerical simulation of flow and heat transfer in fractured crystalline rocks: Application to the hot dry rock site in Rosemanowes. *Geothermics* **1998**, *27*, 1–23. [[CrossRef](#)]
40. Kolditz, O. Modelling flow and heat transfer in fractured rocks: Conceptual model of a 3-D deterministic fracture network. *Geothermics* **1995**, *24*, 451–470. [[CrossRef](#)]
41. Jing, Z.; Willis-Richards, J.; Hashida, K.W. A three-dimensional stochastic rock mechanics model of engineered geothermal systems in fractured crystalline rock. *J. Geophys. Res.* **2000**, *105*, 23663–23679. [[CrossRef](#)]
42. Jing, Z.; Watanabe, K.; Willis-Richards, J.; Hashida, T. A 3-D water/rock chemical interaction model for prediction of HDR/HWR geothermal reservoir performance. *Geothermics* **2002**, *31*, 1–28. [[CrossRef](#)]
43. Jing, Y.N.; Jing, Z.Z.; Willis-Richards, J.; Hashida, T. A simple 3-D thermoelastic model for assessment of the long-term performance of the Hijiori deep geothermal reservoir. *J. Volcanol. Geotherm. Res.* **2014**, *269*, 14–22. [[CrossRef](#)]
44. Baujard, C.; Bruel, D. Numerical study of the impact of fluid density on the pressure distribution and stimulated volume in the Soultz HDR reservoir. *Geothermics* **2006**, *35*, 607–621. [[CrossRef](#)]
45. Sun, Z.X.; Zhang, X.; Xu, Y.; Yao, J.; Wang, H.X.; Lv, S.H.; Sun, Z.L.; Huang, Y.; Cai, M.Y.; Huang, X.X. Numerical simulation of the heat extraction in EGS with thermal-hydraulic-mechanical coupling method based on discrete fractures model. *Energy* **2017**, *120*, 20–33. [[CrossRef](#)]

46. Yao, J.; Zhang, X.; Sun, Z.X.; Huang, Z.Q.; Liu, J.R.; Li, Y.; Xin, Y.; Yan, X.; Liu, W.Z. Numerical simulation of the heat extraction in 3D-EGS with thermal-hydraulic-mechanical coupling method based on discrete fractures model. *Geothermics* **2018**, *74*, 19–34. [[CrossRef](#)]
47. Chen, J.L.; Luo, L.; Jiang, F.M. Analyzing heat extraction and sustainability of EGS with a novel model. *J. Earth Sci. Eng.* **2013**, *3*, 690–700.
48. Chen, J.L.; Jiang, F.M. Designing multi-well layout for enhanced geothermal system to better exploit hot dry rock geothermal energy. *Renew. Energy* **2015**, *74*, 37–48. [[CrossRef](#)]
49. Chen, J.L.; Jiang, F.M. A numerical study of EGS heat extraction process based on a thermal non-equilibrium model for heat transfer in subsurface porous heat reservoir. *Heat Mass Transf.* **2016**, *52*, 255–267. [[CrossRef](#)]
50. Cao, W.J.; Huang, W.B.; Jiang, F.M. Numerical study on variable thermophysical properties of heat transfer fluid affecting EGS heat extraction. *Int. J. Heat Mass Transf.* **2016**, *92*, 1205–1217. [[CrossRef](#)]
51. Cao, W.J.; Huang, W.B.; Jiang, F.M. A novel thermal-hydraulic-mechanical model for the enhanced geothermal system heat extraction. *Int. J. Heat Mass Transf.* **2016**, *100*, 661–671. [[CrossRef](#)]
52. Pruess, K.; Oldenburg, C.; Moridis, G. *TOUGH2 User's Guide, Version 2.0.*; Lawrence Berkeley National Laboratory: Berkeley, CA, USA, 1999.